PERGAMON

International Journal of Solids and Structures 38 (2001) 815–831

INTERNATIONAL JOURNAL OF SOLIDS and STRUCTURES

www.elsevier.com/locate/ijsolstr

On the dynamic behaviour of interacting interfacial cracks in piezoelectric media

X.D. Wang *

Department of Mechanical Engineering, University of Alberta Edmonton, Alberta, Canada T6G 2G8

Received 12 June 1999

Abstract

In this paper, we examine the dynamic electromechanical behaviour of interacting interfacial cracks between two piezoelectric media under antiplane mechanical loading. The cracks are assumed to be permeable, i.e. both the electric potential and the normal electric displacement are continuous across the crack surfaces. The electromechanical field of a single interfacial crack was determined using Fourier transform technique and solving the resulting integral equations. This fundamental solution was then implemented into a pseudo-incident wave method to account for the interaction between different cracks. Typical examples are provided to show the effect of the positioning of the cracks, the material combination and the loading frequency upon the local stress field around the crack tips. The results show the significant effect of an electromechanical coupling upon the stress intensity factors.

Keywords: Interface; Crack; Piezoelectricity; Dynamic behaviour; Interaction

1. Introduction

Since the pioneering work of the Curies in 1880 on Rochelle salt, much attention has been devoted to the characterisation of different piezoelectric materials, especially piezoceramics. Piezoceramic materials have the advantages of quick response, low power consumption, high linearity and a relatively large induced strain for an applied electric field. As a result, they had been used in the design of different smart structures, e.g. large-scale space structures, aircraft structures, satellites, and so forth (Gandhi and Thompson, 1992; Varadan et al., 1993; Mal and Lee, 1993; Ashley, 1995; Dosch et al., 1995). In addition, piezoceramic actuators can be easily fabricated into different desired shapes that can be used in different applications to achieve the highest possible displacement or force for the lowest possible voltage.

One of the most fundamental issues surrounding the effective use of piezoceramic actuators in smart material/structure systems is that piezoceramic materials are usually very brittle. As a result, piezoceramic actuators have a tendency to develop critical cracks during the manufacturing and the poling processes. The

* Tel.: +1-780-492-4517; fax: +1-780-492-2200.
E-mail address: xiaodong.wang@ualberta.ca (X.D. Wang).

0020-7683/01/$ - see front matter
PII: S0020-7683(00)00044-5

existence of these defects will greatly affect the mechanical integrity and electromechanical behaviour of this class of material (Jain and Sirkis, 1994; Park and Sun, 1994). Another important aspect related to the design of the integrated smart structures is the determination of the effect of debonding along the interfaces between piezoelectric actuators/sensors and the host structures. An accurate assessment of the coupled electromechanical behaviour of an integrated structure would, therefore, require the determination of the local stress distribution in the structure involving the interacting cracks and interfaces.

Significant efforts had been made to the study of the quasistatic electromechanical fracture and damage behaviour of piezoelectric materials, for example the work by Pak (1990), Sosa and Pak (1990), Sosa (1991) and Suo et al. (1992), He et al. (1994) and Pak and Goloubeva (1995). In contrast, the dynamic behaviour of cracks in piezoelectric materials has received much less attention, especially when multiple cracks are involved. Existing work has focussed mostly on the dynamic behaviour of a single crack, e.g. the work by Narita and Shindo (1998), Li and Mataga (1996a,b) and Shindo et al. (1996). It should be mentioned, however, that piezoelectric materials are mostly being used or considered for use in situations where dynamic loading is involved, such as the vibration control of smart structures under impact loading and the acoustic control of smart skin systems.

The objective of the present paper is to provide a theoretical treatment of the dynamic interaction between interfacial cracks in piezoelectric media under dynamic antiplane mechanical loading. The current loading condition and configuration represent the effect of the applied mechanical load upon the transverse growth of interfacial debonding between piezoelectric actuators/sensors and the host structures. A permeable crack model is employed in the current study. The theoretical formulations governing the steady-state problem are based upon the use of integral transform techniques and a pseudo-incident wave method. The resulting dynamic stress intensity factors at the interacting cracks are obtained by solving the appropriate singular integral equations using Chebyshev polynomial expansion at different loading frequencies. Numerical examples are provided to show the effect of the geometry of the interacting cracks, the piezoelectric constants of the material and the loading frequency upon the resulting dynamic stress intensity factors.

2. Formulation of the problem

Consider the problem of two bonded infinite piezoelectric materials containing M interfacial cracks subjected to a harmonic incident wave of frequency ω with an incident angle Γ, as shown in Fig. 1. The half-length of crack n is assumed to be a_n. A global Cartesian coordinate system (X, Y) and M local systems (x_n, y_n) $(n = 1, 2, \ldots, M)$ are employed to characterise the different cracks. The position of the centre of crack n is given by $X = X_n$.

The steady-state mechanical and electrical fields corresponding to this incident wave will generally involve an exponential harmonic factor $\exp(-i\omega t)$. For the sake of convenience, this factor will be suppressed and only the amplitude of different field variables will be considered.

The electromechanical behaviour of a homogeneous piezoelectric material under antiplane mechanical and inplane electric loading is fully described, as shown in Appendix A, by the following governing equations:

$$\nabla^2 w + k^2 w = 0, \quad \nabla^2 f = 0, \tag{1}$$

where the Laplacian operator ∇^2 stands for $\partial^2/\partial x^2 + \partial^2/\partial y^2$, and w is the antiplane displacement and k is the wave number defined by

$$k^2 = \frac{\rho\omega^2}{c^*} \quad \text{with } c^* = c_{44} + \frac{e_{15}^2}{\kappa_{11}}. \tag{2}$$

The electric potential ϕ is given by

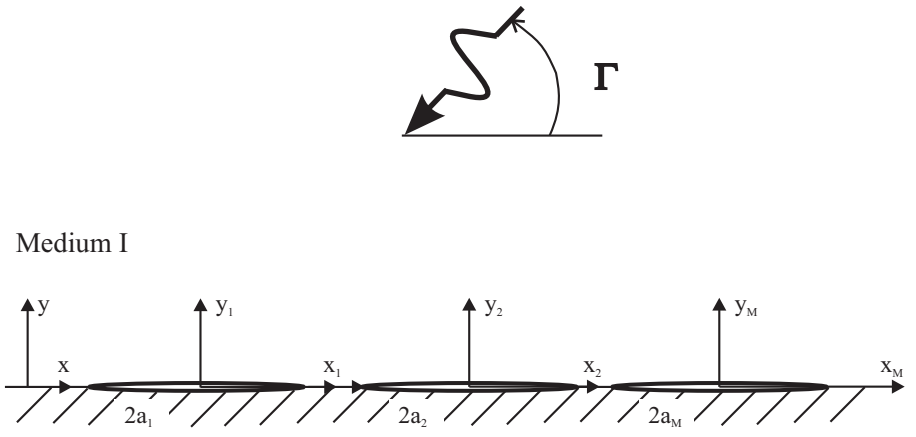

Fig. 1. Interacting cracks between two piezoelectric media.

$$\phi = \frac{e_{15}}{\kappa_{11}} w + f. \tag{3}$$

In the above equations, c_{44}, e_{15} and κ_{11} are the elastic modulus, the piezoelectric constant and the dielectric constant of the medium, respectively.

The corresponding non-vanishing stress and electric displacement components are given by:

$$\tau_{yz} = c^* \frac{\partial w}{\partial y} + e_{15} \frac{\partial f}{\partial y}, \qquad \tau_{xz} = c^* \frac{\partial w}{\partial x} + e_{15} \frac{\partial f}{\partial x}, \tag{4}$$

$$D_x = -\kappa_{11} \frac{\partial f}{\partial x}, \qquad D_y = -\kappa_{11} \frac{\partial f}{\partial y}. \tag{5}$$

For the current non-homogeneous medium, both the upper and lower media are governed by these equations, in which the material constants should be replaced by those of the corresponding media.

3. Solution of single interfacial crack problem

Consider now the steady state antiplane shear problem of a single crack of length $2a$ between two piezoelectric media, as shown in Fig. 2. For the current linear system, the total field can be decomposed into the incident field and the scattering field. The mechanical boundary condition at the surfaces of the crack is assumed to be traction free. Therefore, the scattering field should satisfy the following boundary conditions:

$$w(x,0) = 0 \qquad |x| \geqslant a, \quad \tau_{yz}(x,0+) = \tau_{yz}(x,0-) = -\tau^{\text{in}}(x) \qquad |x| < a. \tag{6}$$

The electric boundary condition of a crack in piezoelectric media had been the topic of many investigations (McMeeking, 1989; Dunn, 1994; Zhang et al., 1998). For this antiplane problem, since no opening

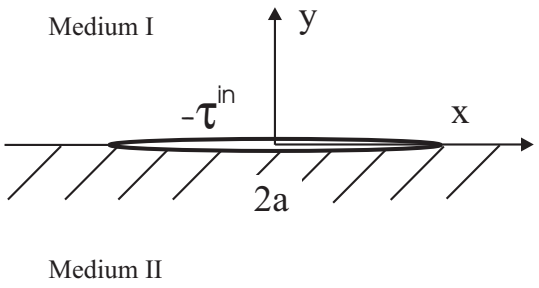

Fig. 2. A single interfacial crack.

displacement exists, the crack surfaces can be assumed to be in perfect contact. Accordingly, permeable condition will be enforced in the current study, i.e., both the electric potential and the normal electric displacement are assumed to be continuous across the crack surfaces, which can be expressed as

$$D_y(x,0+) = D_y(x,0-) \quad \text{and} \quad \phi(x,0+) = \phi(x,0-). \tag{7}$$

The resulting scattering field can be obtained, by solving Eq. (1) using Fourier transform, leading to

$$w(x,y) = \begin{cases} \int_{-\infty}^{\infty} A(s)\,\mathrm{e}^{-\alpha_{\mathrm{I}} y - \mathrm{i}sx}\,\mathrm{d}s, & y > 0 \\ \int_{-\infty}^{\infty} B(s)\,\mathrm{e}^{\alpha_{\mathrm{II}} y - \mathrm{i}sx}\,\mathrm{d}s, & y < 0, \end{cases} \tag{8}$$

$$f(x,y) = \begin{cases} \int_{-\infty}^{\infty} C(s)\,\mathrm{e}^{-|s|y - \mathrm{i}sx}\,\mathrm{d}s, & y > 0, \\ \int_{-\infty}^{\infty} D(s)\,\mathrm{e}^{|s|y - \mathrm{i}sx}\,\mathrm{d}s, & y < 0, \end{cases} \tag{9}$$

where $A(s)$, $B(s)$, $C(s)$ and $D(s)$ are unknown functions of s and α_{I} and α_{II} are given by

$$\alpha_{\mathrm{I}} = \begin{cases} \sqrt{s^2 - k_{\mathrm{I}}^2}, & |s| \geqslant k_{\mathrm{I}}, \\ -\mathrm{i}\sqrt{k_{\mathrm{I}}^2 - s^2}, & |s| < k_{\mathrm{I}}, \end{cases} \qquad \alpha_{\mathrm{II}} = \begin{cases} \sqrt{s^2 - k_{\mathrm{II}}^2}, & |s| \geqslant k_{\mathrm{II}}, \\ -\mathrm{i}\sqrt{k_{\mathrm{II}}^2 - s^2}, & |s| < k_{\mathrm{II}}. \end{cases} \tag{10}$$

It should be noted that the scattering field given by Eqs. (8) and (9) satisfies the zero-stress and zero-electric displacement conditions of the scattering field at infinity.

By using the continuity conditions of electric displacement D_y, electric potential ϕ and shear stress τ_{yz} across the interface, $A(s)$, $B(s)$, $C(s)$ and $D(s)$ can be expressed in terms of one unknown function $E(s)$ as

$$A(s) = -\frac{\Delta_1(s)}{\Delta(s)}E(s), \qquad B(s) = \frac{\Delta_2(s)}{\Delta(s)}E(s), \tag{11}$$

$$C(s) = \kappa_{11}^{\mathrm{II}} E(s), \qquad D(s) = -\kappa_{11}^{\mathrm{I}} E(s) \tag{12}$$

where Δ_1, Δ_2 and Δ are given by

$$\Delta_1(s) = (\kappa_{11}^{\mathrm{I}} + \kappa_{11}^{\mathrm{II}})c^{*\mathrm{II}}\alpha_{\mathrm{II}} + |s|\left(e_{15}^{\mathrm{I}} e_{15}^{\mathrm{II}} - e_{15}^{\mathrm{II}2}\frac{\kappa_{11}^{\mathrm{I}}}{\kappa_{11}^{\mathrm{II}}}\right), \tag{13}$$

$$\Delta_2(s) = (\kappa_{11}^{\mathrm{I}} + \kappa_{11}^{\mathrm{II}})c^{*\mathrm{I}}\alpha_{\mathrm{I}} + |s|\left(e_{15}^{\mathrm{I}} e_{15}^{\mathrm{II}} - e_{15}^{\mathrm{I}2}\frac{\kappa_{11}^{\mathrm{II}}}{\kappa_{11}^{\mathrm{I}}}\right), \tag{14}$$

$$\Delta(s) = \frac{e_{15}^{\mathrm{I}}}{\kappa_{11}^{\mathrm{I}}}c^{*\mathrm{II}}\alpha_{\mathrm{II}} + \frac{e_{15}^{\mathrm{II}}}{\kappa_{11}^{\mathrm{II}}}c^{*\mathrm{I}}\alpha_{\mathrm{I}}. \tag{15}$$

In these expressions, the superscripts (subscripts) 'I' and 'II' represent the upper and lower media, respectively.

$E(s)$ can further be expressed in terms of the following unknown dislocation density function:

$$\psi(x) = \frac{\partial[w(x,0^+) - w(x,0^-)]}{\partial x}, \quad |x| \leqslant a \tag{16}$$

as

$$E(s) = -\frac{\mathrm{i}}{2\pi s}\frac{\Delta}{\Delta_1 + \Delta_2}\int_{-\infty}^{\infty}\psi(x)\mathrm{e}^{\mathrm{i}sx}\,\mathrm{d}x. \tag{17}$$

The stress distribution along the interface can then be obtained by using Eq. (4),

$$\tau_{yz}(x,0) = \int_{-a}^{a}\psi(u)\int_{-\infty}^{\infty}\frac{\mathrm{i}G(s)}{2\pi s}\mathrm{e}^{\mathrm{i}s(u-x)}\,\mathrm{d}s\,\mathrm{d}u, \tag{18}$$

where $G(s)$ is given by

$$G(s) = \frac{g(s)}{\Delta_1(s) + \Delta_2(s)} \tag{19}$$

with

$$g(s) = -(\kappa_{11}^{\mathrm{I}} + \kappa_{11}^{\mathrm{II}})c^{*\mathrm{I}}c^{*\mathrm{II}}\alpha_{\mathrm{I}}\alpha_{\mathrm{II}} + \left(c^{*\mathrm{I}}\alpha_{\mathrm{I}}e_{15}^{\mathrm{II}2}\frac{\kappa_{11}^{\mathrm{I}}}{\kappa_{11}^{\mathrm{II}}} + c^{*\mathrm{II}}\alpha_{\mathrm{II}}e_{15}^{\mathrm{I}2}\frac{\kappa_{11}^{\mathrm{II}}}{\kappa_{11}^{\mathrm{I}}}\right)|s|. \tag{20}$$

The kernel of the infinite integration in Eq. (18) tends to a constant when $|s| \to \infty$, which corresponds to the singular term of the stress component. After performing the appropriate asymptotic analysis, the following result can be obtained:

$$\beta_0 = -\lim_{s\to\infty}\frac{G(s)}{s} = \frac{(\kappa_{11}^{\mathrm{I}} + \kappa_{11}^{\mathrm{II}})c^{*\mathrm{I}}c^{*\mathrm{II}} - c^{*\mathrm{I}}e_{15}^{\mathrm{II}2}\frac{\kappa_{11}^{\mathrm{I}}}{\kappa_{11}^{\mathrm{II}}} - c^{*\mathrm{II}}e_{15}^{\mathrm{I}2}\frac{\kappa_{11}^{\mathrm{II}}}{\kappa_{11}^{\mathrm{I}}}}{(\kappa_{11}^{\mathrm{I}} + \kappa_{11}^{\mathrm{II}})(c^{*\mathrm{I}} + c^{*\mathrm{II}}) + \left(2e_{15}^{\mathrm{I}}e_{15}^{\mathrm{II}} - e_{15}^{\mathrm{I}2}\frac{\kappa_{11}^{\mathrm{II}}}{\kappa_{11}^{\mathrm{I}}} - e_{15}^{\mathrm{II}2}\frac{\kappa_{11}^{\mathrm{I}}}{\kappa_{11}^{\mathrm{II}}}\right)}. \tag{21}$$

By substituting Eq. (18) and (16) into Eq. (6) and making use of the asymptotic behaviour of the problem given by Eq. (21), a system of governing equations for determining ψ are obtained in terms of the following singular integral equations:

$$\int_{-a}^{a}\frac{\psi(u)}{u-x}\,\mathrm{d}u - \int_{-a}^{a}\psi(u)\int_{0}^{\infty}\left(\frac{G(s)}{\beta_0 s} + 1\right)\sin[s(u-x)]\,\mathrm{d}s\,\mathrm{d}u = -\frac{\pi}{\beta_0}\tau^{\mathrm{in}}(x), \quad |x| < a \tag{22}$$

and

$$\int_{-a}^{a}\psi(u)\,\mathrm{d}u = 0. \tag{23}$$

Eq. (22) is a first kind of singular integral equation. The solution of it includes the well-known square-root singularity and can be expressed as

$$\psi(u) = \sum_{j=0}^{\infty}\frac{c_j}{\sqrt{1 - \frac{u^2}{a^2}}}T_j\left(\frac{u}{a}\right) \tag{24}$$

where T_j are Chebyshev polynomials of the first kind and c_j are unknown constants. From the orthogonality conditions of Chebyshev polynomials, Eq. (23) leads to $c_0 = 0$. Substituting Eq. (24) into Eq. (22), the following algebraic equation for c_j is obtained:

$$\sum_{j=1}^{\infty} c_j U_{j-1}\left(\frac{x}{a}\right) - \sum_{j=1}^{\infty} c_j g_j(x) = -\frac{1}{\beta_0}\tau^{\text{in}}(x), \quad |x| < a \tag{25}$$

where U_j represents Chebyshev polynomial of the second kind with

$$g_j(x) = \begin{cases} (-1)^p a \int_0^\infty \left(\frac{G(s)}{\beta_0 s} + 1\right) J_j(sa)\cos(sx)\,\mathrm{d}s, & j = 2p+1, \\ (-1)^{(p+1)} a \int_0^\infty \left(\frac{G(s)}{\beta_0 s} + 1\right) J_j(sa)\sin(sx)\,\mathrm{d}s, & j = 2p \end{cases} \tag{26}$$

in which J_j is the Bessel function of the first kind. Truncating the Chebyshev polynomials in Eq. (24) to the Nth term and assuming that Eq. (25) is satisfied at N collocation points along the crack surface,

$$x_l = a\cos\left(\frac{l}{N+1}\pi\right), \quad l = 1, 2, \ldots, N, \tag{27}$$

Eq. (25) can be reduced to a linear algebraic system of equations of the following form:

$$\sum_{j=1}^{N} c_j \frac{\sin\left(\frac{jl\pi}{N+1}\right)}{\sin\left(\frac{j\pi}{N+1}\right)} - \sum_{j=1}^{N} c_j g_j(x_l) = -\frac{1}{\beta_0}\tau^{\text{in}}(x_l), \quad j, l = 1, 2, \ldots, N. \tag{28}$$

The solution of c_j can then be obtained by solving the following equation:

$$[A]\{c\} = -\{t\}/\beta_0, \tag{29}$$

where

$$\{c\} = [c_1, c_2, \ldots, c_j, \ldots, c_N]^{\mathrm{T}}, \tag{30}$$

$$\{t\} = [\tau^{\text{in}}(x_1), \tau^{\text{in}}(x_2), \ldots, \tau^{\text{in}}(x_N)]^{\mathrm{T}}, \tag{31}$$

and,

$$[A] = \begin{bmatrix} A_{11} & A_{12} & \ldots & A_{1N} \\ A_{21} & A_{22} & \ldots & A_{2N} \\ \vdots & \vdots & \vdots & \vdots \\ A_{N1} & A_{N2} & \ldots & A_{NN} \end{bmatrix} \tag{32}$$

with

$$A_{lj} = \frac{\sin\left(\frac{jl\pi}{N+1}\right)}{\sin\left(\frac{j\pi}{N+1}\right)} - g_j(x_l), \quad j, l = 1, 2, \ldots, N. \tag{33}$$

Based on the solution given by Eq. (29), the stress distribution along the interface resulting from the current crack can be obtained by substituting Eq. (24) into Eq. (18), such that

$$\tau_{yz}(x, 0) = [f(a, x)]\{c\} \tag{34}$$

in which $[f(a,x)] = [f_1(a,x),\ f_2(a,x), \ldots,\ f_N(a,x)]$ and $f_j(a,x)$ $(j = 1, 2, \ldots, N)$ are given by

$$f_j(a,x)=\begin{cases}(-1)^p a\int_0^\infty \beta_0 J_j(sa)\cos(sx)\,\mathrm{d}s, & j=2p+1\\ (-1)^{(p+1)} a\int_0^\infty \beta_0 J_j(sa)\sin(sx)\,\mathrm{d}s, & j=2p\end{cases} \tag{35}$$

$$-\begin{cases}(-1)^p a\int_0^\infty \left[\frac{G(s)}{s}+\beta_0\right]J_j(sa)\cos(sx)\,\mathrm{d}s, & j=2p+1,\\ (-1)^{(p+1)} a\int_0^\infty \left[\frac{G(s)}{s}+\beta_0\right]J_j(sa)\sin(sx)\,\mathrm{d}s, & j=2p,\end{cases}$$

where

$$\int_0^\infty J_j(sa)\cos(sx)\,\mathrm{d}s=\frac{(-1)^{p+1}a^j}{\sqrt{x^2-a^2}\left[\sqrt{x^2-a^2}+|x|\right]^j},\quad j=2p+1, \tag{36}$$

$$\int_0^\infty J_j(sa)\sin(sx)\,\mathrm{d}s=\mathrm{sgn}(x)\frac{(-1)^{p+1}a^j}{\sqrt{x^2-a^2}\left[\sqrt{x^2-a^2}+|x|\right]^j},\quad j=2p. \tag{37}$$

4. Interaction between cracks

For the general cases where multiple interface cracks are involved, as shown in Fig. 1, the interaction between these cracks may significantly affect the local stress field around the crack tips. This interaction effect will be considered in this section using a pseudo-incident wave method based on the single interfacial crack solution.

4.1. Pseudo-incident wave method

Let us now focus our attention on crack n. In addition to the original incident wave τ^0, the crack will experience scattering waves from other cracks as depicted in Fig. 3. In this case, the effect of other cracks upon crack n can be regarded as an unknown incident wave, pseudo-incident wave τ_n^{p}. Accordingly, the behaviour of crack n can be equivalently described by a single interfacial crack between two bonded infinite piezoelectric media subjected to an incident wave given by

$$\tau_n^{\mathrm{in}}=\tau^0+\tau_n^{\mathrm{p}}. \tag{38}$$

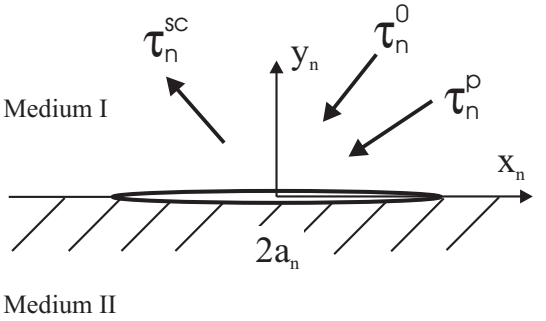

Fig. 3. A single crack subjected to a pseudo-incident wave.

In response to this incident wave, crack n will result in a scattering wave τ_n^{sc}. The total stress field in the matrix can then be expressed as

$$\tau^{total} = \tau^0 + \tau_n^p + \tau_n^{sc}. \tag{39}$$

The total stress field in the matrix can also be obtained by summing up the initial field and the contributions from all the cracks to give

$$\tau^{total} = \tau^0 + \sum_{m=1}^{M} \tau_m^{sc}. \tag{40}$$

The equivalence between Eqs. (39) and (40) indicates that

$$\tau_n^p = \sum_{m\neq n}^{M} \tau_m^{sc}, \quad n = 1, 2, \ldots, M. \tag{41}$$

Eq. (41) represents the relation between the different cracks.

4.2. Solution of interacting cracks

Based on the single interfacial crack solution discussed in Section 3, the interfacial stress at point X due to crack m can be expressed, by using Eq. (34), as

$$\tau_m^{sc}(X) = [f(a_m, X - X_m)]\{c\}^m, \tag{42}$$

where $\{c\}^m$ is the coefficient of Chebyshev polynomial expansion of crack m.

For any crack n, the interfacial stress acting on its surfaces induced by the pseudo-incident wave can be obtained by substituting Eq. (42) into Eq. (41) as

$$\tau_n^p(x_n) = \sum_{m\neq n}^{M} [f(a_m, x_n - X_m + X_n)]\{c\}^m. \tag{43}$$

We are interested in the shear stress at the following collocation points:

$$x_n^l = a_n \cos\left(\frac{l}{N+1}\pi\right), \quad l = 1, 2, \ldots, N. \tag{44}$$

By using Eqs. (43), (44) and (38), the stress at these points due to the total incident wave of crack n can be obtained as

$$\{t\}_n = \{t\}_n^0 + [Q]^n\{C\} \tag{45}$$

where

$$\{t\}_n^0 = \begin{Bmatrix} \tau^0(x_n^1) \\ \tau^0(x_n^2) \\ \vdots \\ \tau^0(x_n^N) \end{Bmatrix}, \quad \{C\} = \begin{Bmatrix} \{c\}^1 \\ \{c\}^2 \\ \vdots \\ \{c\}^M \end{Bmatrix} \tag{46}$$

with $\{t\}_n^0$ being the stress due to the initial incident wave and $\{C\}$ being the coefficients of the Chebyshev polynomial expansion of the interacting cracks. $[Q]^n$ represents the interaction between cracks and is given by

$$[Q]^n = \begin{bmatrix} 0 & \left[f\left(a_2, x_n^1 - X_2 + X_n\right)\right] & \dots & \left[f\left(a_M, x_n^1 - X_M + X_n\right)\right] \\ \left[f\left(a_1, x_n^2 - X_1 + X_n\right)\right] & 0 & \dots & \left[f\left(a_M, x_n^2 - X_M + X_n\right)\right] \\ & & \dots & \\ \left[f\left(a_1, x_n^N - X_1 + X_n\right)\right] & \left[f\left(a_2, x_n^N - X_2 + X_n\right)\right] & \dots & 0 \end{bmatrix}. \tag{47}$$

Therefore, by using Eqs. (45) and (29), the Chebyshev polynomial expansion coefficients of crack n, $\{c\}^n = \{c_1^n, c_2^n, \dots, c_N^n\}^{\mathrm{T}}$, can be determined by

$$[A]^n\{c\}^n = -(\{t\}_n^0 + [Q]^n\{C\})/\beta_0. \tag{48}$$

$[A]^n$ is a known matrix which is given by Eq. (32) with half the length of the crack a being replaced by a_n. By substituting Eq. (47) into Eq. (48), the governing equation for solving $\{C\}$ can be obtained as

$$\left\{ \begin{bmatrix} [A]^1 & 0 & \dots & 0 \\ 0 & [A]^2 & \dots & 0 \\ 0 & \dots & & 0 \\ 0 & 0 & 0 & [A]^M \end{bmatrix} + \frac{1}{\beta_0} \begin{bmatrix} [Q]^1 \\ [Q]^2 \\ \vdots \\ [Q]^M \end{bmatrix} \right\} \{C\} = -\frac{1}{\beta_0} \begin{Bmatrix} \{t\}_1^0 \\ \{t\}_2^0 \\ \vdots \\ \{t\}_M^0 \end{Bmatrix} \tag{49}$$

from which $\{C\}$ can be determined.

The singular behaviour of the interfacial crack n is characterised by the following stress intensity factors:

$$K_r^n = \lim_{x_n \to a} \left[\sqrt{2\pi(a - x_n)}\tau_{yz}(x_n)\right],$$
$$K_l^n = \lim_{x_n \to -a} \left[\sqrt{2\pi(a + x_n)}\tau_{yz}(x_n)\right]. \tag{50}$$

By using Eq. (34), the stress intensity factor at the right tip of crack n can be expressed in terms of c_j^n as being

$$K_{\mathrm{III}}^n = \sqrt{a_n \pi} \sum_{j=1}^{N} c_j^n. \tag{51}$$

5. Results and discussion

The incident wave considered is a harmonic wave directed at an angle Γ with the interface, as shown in Fig. 4. The incident antiplane displacement and the electric potential can be generally expressed as

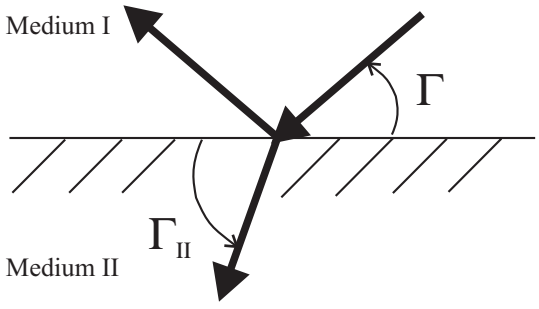

Fig. 4. The reflected and transmitted waves of an interface.

$$w^{(\mathrm{in})} = \overline{w}\mathrm{e}^{-\mathrm{i}k_{\mathrm{I}}(x\cos\Gamma + y\sin\Gamma)}, \quad \phi^{(\mathrm{in})} = \overline{\phi}\mathrm{e}^{-\mathrm{i}k_{\mathrm{I}}(x\cos\Gamma + y\sin\Gamma)}. \tag{52}$$

This incident wave will result in a reflected wave and a transmitted wave in the upper and the lower media, respectively. The resulting interfacial stress can be expressed as

$$\tau_{yz}(X,0) = \tau\sin\Gamma_{\mathrm{II}}\mathrm{e}^{-\mathrm{i}k_{\mathrm{II}}X\cos\Gamma_{\mathrm{II}}}, \tag{53}$$

where τ is the maximum value of the shear stress corresponding to the transmitted wave given in Appendix B and Γ_{II} can be determined by

$$k_{\mathrm{I}}\cos\Gamma = k_{\mathrm{II}}\cos\Gamma_{\mathrm{II}}. \tag{54}$$

The shear stress given by Eq. (53) was used in Eq. (49) as the boundary traction at the crack surfaces in the determination of the scattering field. It should be recognised that the dynamic stress intensity factor produced by a time-harmonic loading is in general a complex quantity. For convenience, however, only the amplitude of the complex dynamic stress intensity factor is considered in the following examples.

5.1. Effect of electromechanical coupling

First, we restrict our attention to the case where the upper and lower materials are identical. Fig. 5 shows the effect of the frequency (k_0a) and piezoelectric constant upon the normalised dynamic stress intensity factor ($K^* = K_{\mathrm{III}}/\tau\sqrt{\pi a}$) of a single crack of length $2a$ due to a normal incident wave ($\Gamma = 90^\circ$) with

$$\lambda = \frac{e_{15}^2}{\kappa_{11}c_{44}}. \tag{55}$$

In this figure, $k_0 = \omega\sqrt{\rho/c_{44}}$ is a wave number with ρ being the mass density of the medium. When the frequency of the incident wave is low ($k_0a < 0.25$), the effect of piezoelectricity is negligible. However, when the frequency k_0a approaches 1.1, the dynamic overshoot phenomenon observed in traditional materials

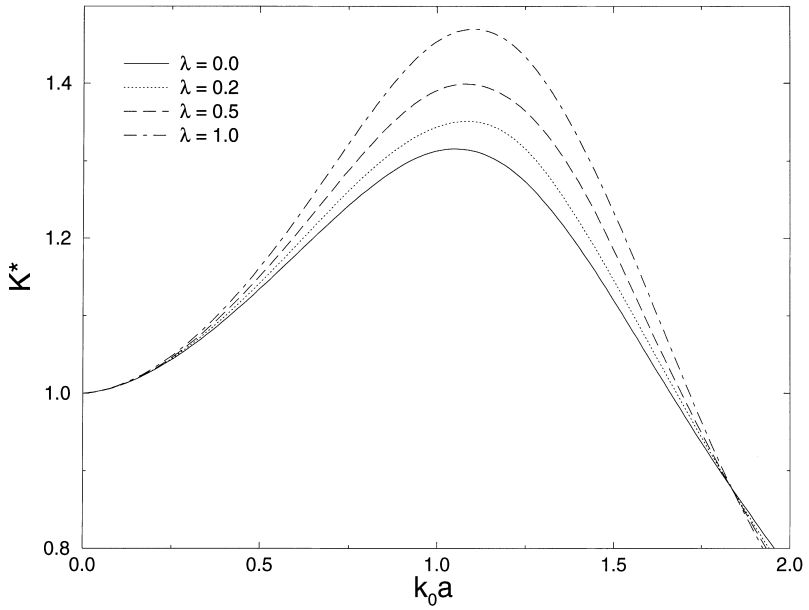

Fig. 5. The effect of the piezoelectric constant upon the dynamic stress intensity factor of a single crack.

(Wang and Meguid, 1997) is significantly intensified. This is due to the coupling between the electric and the mechanical fields.

Fig. 6 shows the normalised stress intensity factor at the inner tips of two collinear cracks of equal length ($2a$) in a homogeneous piezoelectric medium due to a normal incident wave ($\Gamma = 90^\circ$) for the case where the distance between the two cracks is $0.3a$. Similar to the single crack problem, a significant increase in the dynamic stress intensity factor is observed when $k_0 a = 0.7$. In comparison with the corresponding results for traditional materials, the present result indicates that the piezoelectric effect will increase the sensitivity of the stress intensity factor to the frequency of the incident wave.

5.2. Effect of the interface

The normalised stress intensity factor K^* at the inner tips of two interacting interfacial cracks of equal length ($2a$) due to a normal incident wave is depicted in Fig. 7, in which $k_0 = \omega\sqrt{\rho^{\mathrm{I}}/c_{44}^{\mathrm{I}}}$ with ρ^{I} being the mass density of the upper medium and c_{I}^* and c_{II}^* being the effective moduli of the upper and the lower media defined in Eq. (2). It is assumed that the distance between the cracks is $0.3a$, $e_{15}^{\mathrm{I}} = e_{15}^{\mathrm{II}} = 0$ and $\rho^{\mathrm{I}} = \rho^{\mathrm{II}}$ with ρ^{II} being the mass density of the lower medium. The result indicates that the increase of the material mismatch will result in the occurrence of the maximum stress intensity factor at lower frequencies. However, no significant change of the value of the maximum stress intensity factor with the increase of the material mismatch is observed.

Fig. 8 shows the effect of piezoelectric constants upon the stress intensity factor at the inner tips of two identical cracks due to a normal incident wave, for the case where the distance between the cracks is $0.3a$, $\lambda_{\mathrm{II}} = 1$, $c_{44}^{\mathrm{I}} = c_{44}^{\mathrm{II}}$, $\rho^{\mathrm{I}} = \rho^{\mathrm{II}}$ and $\kappa_{11}^{\mathrm{I}} = \kappa_{11}^{\mathrm{II}}$, with λ_{I} and λ_{II} being given by

$$\lambda_{\mathrm{I}} = \frac{e_{15}^{\mathrm{I}2}}{c_{44}^{\mathrm{I}}\kappa_{11}^{\mathrm{I}}}, \quad \lambda_{\mathrm{II}} = \frac{e_{15}^{\mathrm{II}2}}{c_{44}^{\mathrm{II}}\kappa_{11}^{\mathrm{II}}}. \tag{56}$$

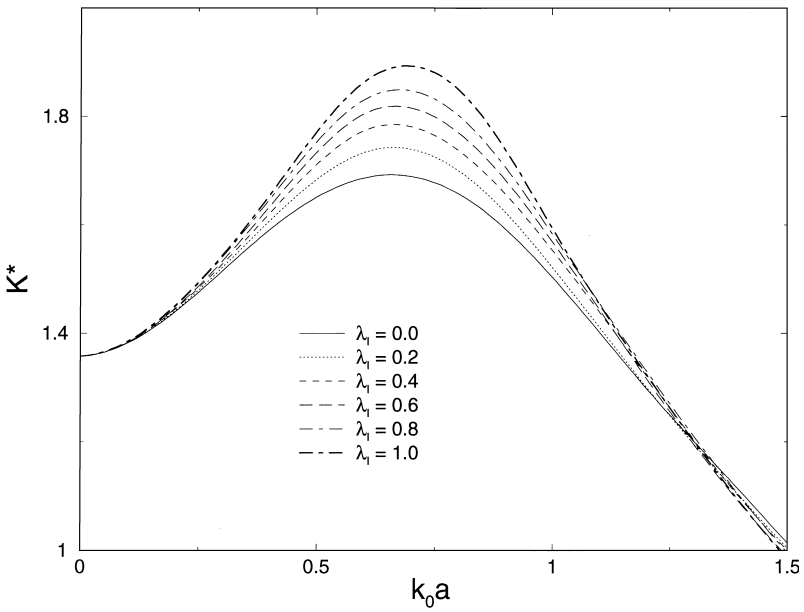

Fig. 6. The effect of the piezoelectric constant upon the dynamic stress intensity factor of interacting cracks.

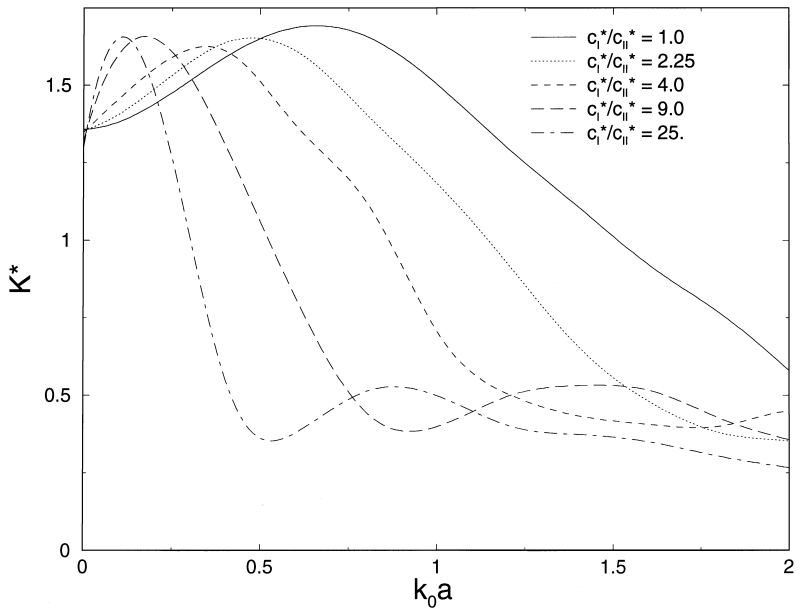

Fig. 7. The effect of the material mismatch upon the dynamic stress intensity factor of interacting interfacial cracks.

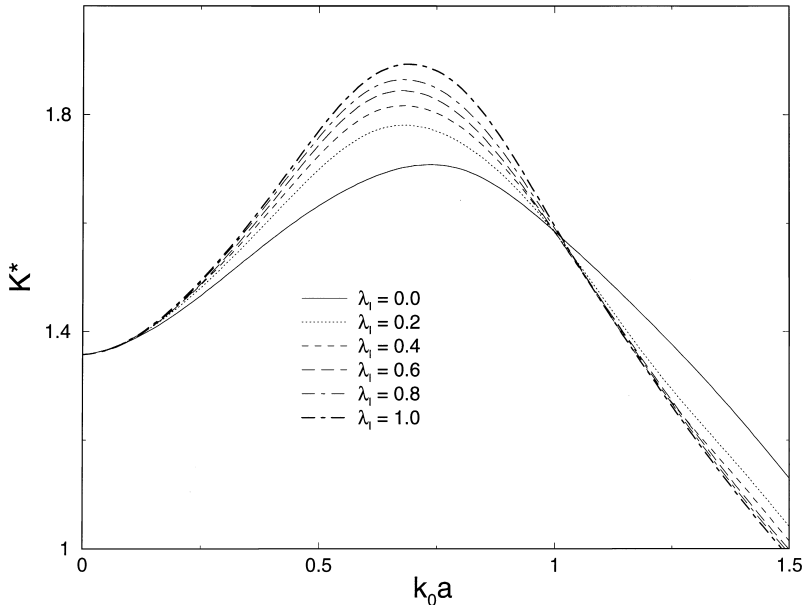

Fig. 8. The dynamic stress intensity factor of interacting interfacial cracks due to a normal incident wave.

It is interesting to notice that the increase of λ_I results in an increase in the stress intensity factor comparable to that for the homogeneous medium shown in Fig. 6.

Fig. 9 shows the dynamic stress intensity factor for the case considered in Fig. 8 under an oblique incident wave ($\Gamma = 45°$). A dramatic effect of the piezoelectric constant upon the stress intensity factor is

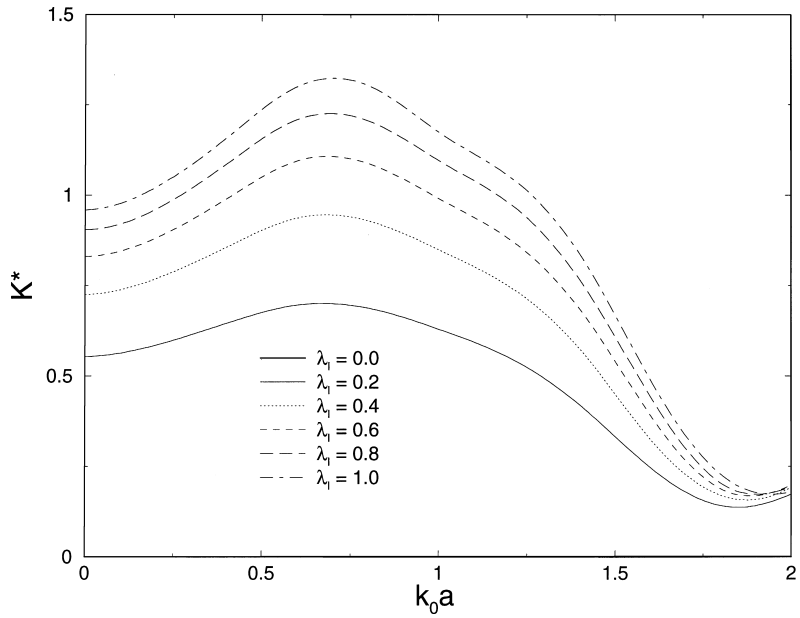

Fig. 9. The dynamic stress intensity factor of interacting interfacial cracks due to an oblique incident wave.

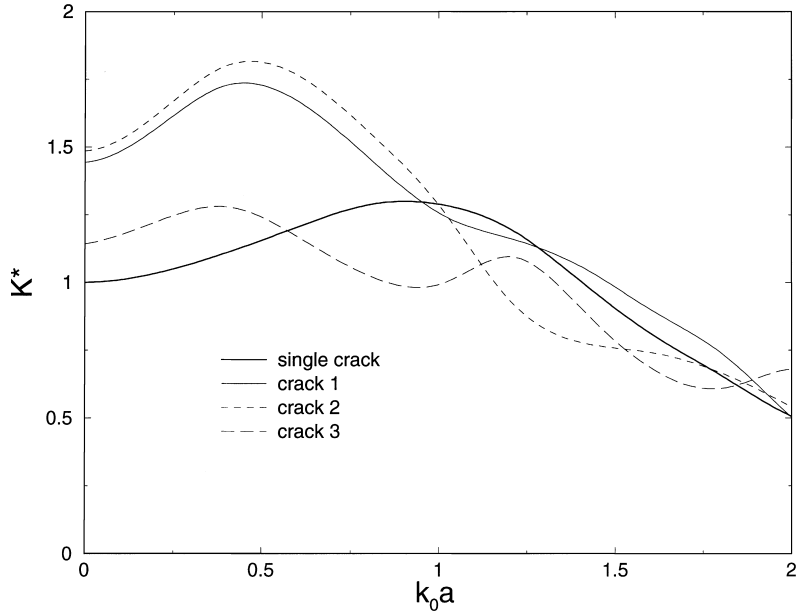

Fig. 10. The dynamic stress intensity factor of three interacting interfacial cracks.

observed. For the limiting case where $\lambda_I = 0$, the current incident wave will not produce a non-zero interfacial stress and therefore results in a zero stress intensity factor at the crack tips.

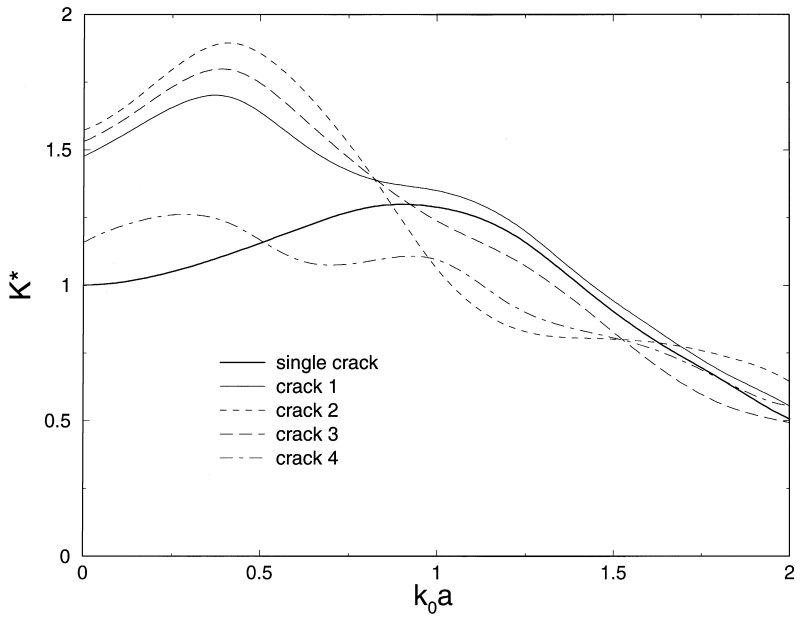

Fig. 11. The dynamic stress intensity factor of four interacting interfacial cracks.

5.3. Multiple interacting cracks

Fig. 10 shows the dynamic stress intensity factors at the right tips of three identical cracks of length $2a$ due to a normal incident wave, for the case where $\lambda_{\mathrm{I}} = 0$, $\lambda_{\mathrm{II}} = 1$, $c_{44}^{\mathrm{I}} = c_{44}^{\mathrm{II}}$, $\rho^{\mathrm{I}} = \rho^{\mathrm{II}}$ and $\kappa_{11}^{\mathrm{I}} = \kappa_{11}^{\mathrm{II}}$. The centres of these cracks are located at $X = 0$, $X = 2.3a$, $X = 4.6a$, respectively. The corresponding single crack solution is also depicted in the same figure for comparison. The stress intensity factor of crack three is fairly close to that of the single crack. However, the stress intensity factors at the inner tips (crack one and crack two) show significant difference from the single crack solution.

The corresponding result of four identical interacting cracks is shown in Fig. 11, where the centres of the cracks are assumed to be $X = 0$, $X = 2.3a$, $X = 4.6a$, $X = 6.9a$, respectively. Compared to the result of the three-crack case shown in Fig. 10, the stress intensity factors at the inner and outer tips show no significant difference until $k_0 a$ approaches 0.8.

6. Concluding remarks

A general solution is provided to the dynamic interaction between interfacial cracks between two piezoelectric media under antiplane mechanical and inplane electrical loading. The analysis is based on the use of integral transform techniques and integral equation methods coupled with a pseudo-incident wave method. Attention has been focussed on the study of the fundamental behaviour of the local stress field around the crack tips. The effect of the geometry of the cracks, the material constants and the frequency of the incident wave upon the dynamic stress intensity factor is examined and discussed. The study reveals the importance of the electromechanical coupling terms upon the resulting dynamic stress intensity factors.

Acknowledgements

This work was supported by the Research Excellence Envelope program at the University of Alberta.

Appendix A

The equilibrium equation and Gauss' law for a piezoelectric medium under antiplane loading are given by

$$\frac{\partial \tau_{xz}}{\partial x}+\frac{\partial \tau_{yz}}{\partial y}+\rho\omega^2 w=0,$$

$$\frac{\partial D_x}{\partial x}+\frac{\partial D_y}{\partial y}=0$$

in which τ_{xz} and τ_{yz} are the shear stress components, D_x and D_y are the electric displacements, while w, ρ and ω are the antiplane displacement, mass density and frequency, respectively. Most existing piezoceramics are transversely isotropic, with the axis of symmetry being along the poling direction of the material. If the z-axis is chosen to be along this direction, the non-vanishing stress components (τ_{xz} and τ_{yz}) and the electric displacements (D_x and D_y) can be expressed as

$$\tau_{xz}=c_{44}\frac{\partial w}{\partial x}+e_{15}\frac{\partial \phi}{\partial x},\qquad \tau_{yz}=c_{44}\frac{\partial w}{\partial y}+e_{15}\frac{\partial \phi}{\partial y},$$

and

$$D_x=e_{15}\frac{\partial w}{\partial x}-\kappa_{11}\frac{\partial \phi}{\partial x},\qquad D_y=e_{15}\frac{\partial w}{\partial y}-\kappa_{11}\frac{\partial \phi}{\partial y}$$

where ϕ is the electric potential, c_{44}, e_{15} and κ_{11} are the elastic modulus, the piezoelectric constant and the dielectric constant of the medium, respectively. Substituting the constitutive equations into the equilibrium equation and Gauss' law results in

$$\nabla^2 w+k^2 w=0,\quad \nabla^2 f=0,$$

where k is the wave number defined in Eq. (2).

Appendix B

Consider an incident wave directed at an angle Γ with the interface, as shown in Fig. 4, given by

$$w^{(\mathrm{in})}=\overline{w}\mathrm{e}^{-\mathrm{i}k_{\mathrm{I}}(x\cos\Gamma+y\sin\Gamma)},\qquad \phi^{(\mathrm{in})}=\overline{\phi}\mathrm{e}^{-\mathrm{i}k_{\mathrm{I}}(x\cos\Gamma+y\sin\Gamma)}.$$

The resulting reflected and transmitted waves in the upper and the lower media can be expressed as

$$w^{(\mathrm{re})}=\overline{w}_{\mathrm{I}}\mathrm{e}^{-\mathrm{i}k_{\mathrm{I}}(x\cos\Gamma+y\sin\Gamma)},\qquad \phi^{(\mathrm{re})}=\overline{\phi}_{\mathrm{I}}\mathrm{e}^{-\mathrm{i}k_{\mathrm{I}}(x\cos\Gamma+y\sin\Gamma)},$$

$$w^{(\mathrm{tr})}=\overline{w}_{\mathrm{II}}\mathrm{e}^{-\mathrm{i}k_{\mathrm{II}}(x\cos\Gamma_{\mathrm{II}}+y\sin\Gamma_{\mathrm{II}})},\qquad \phi^{(\mathrm{tr})}=\overline{\phi}_{\mathrm{II}}\mathrm{e}^{-\mathrm{i}k_{\mathrm{II}}(x\cos\Gamma_{\mathrm{II}}+y\sin\Gamma_{\mathrm{II}})}$$

in which

$$\Gamma_{\mathrm{I}}=\Gamma,\qquad k_{\mathrm{I}}\cos\Gamma=k_{\mathrm{II}}\cos\Gamma_{\mathrm{II}},$$

$$\overline{w}_{\mathrm{II}}=\overline{w}+\overline{w}_{\mathrm{I}},\qquad \overline{\phi}_{\mathrm{II}}=\overline{\phi}+\overline{\phi}_{\mathrm{I}}$$

with

$$\overline{w}_{\mathrm{I}} = (F_1\overline{w} + F_2\overline{\phi})/F, \qquad \overline{\phi}_{\mathrm{I}} = (F_3\overline{w} + F_4\overline{\phi})/F$$

and

$$\begin{aligned}
F_1 = & -(k_{\mathrm{II}}\sin\Gamma_{\mathrm{II}}\kappa_{11}^{\mathrm{II}} + \kappa_{11}^{\mathrm{I}}k_{\mathrm{I}}\sin\Gamma)(c_{44}^{\mathrm{I}}k_{\mathrm{I}}\sin\Gamma - k_{\mathrm{II}}\sin\Gamma_{\mathrm{II}}c_{44}^{\mathrm{II}}) \\
& -(k_{\mathrm{II}}\sin\Gamma_{\mathrm{II}}e_{15}^{\mathrm{II}} + e_{15}^{\mathrm{I}}k_{\mathrm{I}}\sin\Gamma)(k_{\mathrm{II}}\sin\Gamma_{\mathrm{II}}e_{15}^{\mathrm{II}} - e_{15}^{\mathrm{I}}k_{\mathrm{I}}\sin\Gamma), \\
F_2 = & -(k_{\mathrm{II}}\sin\Gamma_{\mathrm{II}}\kappa_{11}^{\mathrm{II}} + \kappa_{11}^{\mathrm{I}}k_{\mathrm{I}}\sin\Gamma)(e_{15}^{\mathrm{I}}k_{\mathrm{I}}\sin\Gamma - e_{15}^{\mathrm{II}}k_{\mathrm{II}}\sin\Gamma_{\mathrm{II}}) \\
& +(k_{\mathrm{II}}\sin\Gamma_{\mathrm{II}}\kappa_{11}^{\mathrm{II}} - \kappa_{11}^{\mathrm{I}}k_{\mathrm{I}}\sin\Gamma)(k_{\mathrm{II}}\sin\Gamma_{\mathrm{II}}e_{15}^{\mathrm{II}} + e_{15}^{\mathrm{I}}k_{\mathrm{I}}\sin\Gamma), \\
F_3 = & (k_{\mathrm{II}}\sin\Gamma_{\mathrm{II}}e_{15}^{\mathrm{II}} - e_{15}^{\mathrm{I}}k_{\mathrm{I}}\sin\Gamma)(k_{\mathrm{II}}\sin\Gamma_{\mathrm{II}}c_{44}^{\mathrm{II}} + k_{\mathrm{I}}\sin\Gamma c_{44}^{\mathrm{I}}) \\
& -(c_{44}^{\mathrm{I}}k_{\mathrm{I}}\sin\Gamma - k_{\mathrm{II}}\sin\Gamma_{\mathrm{II}}c_{44}^{\mathrm{II}})(k_{\mathrm{II}}\sin\Gamma_{\mathrm{II}}e_{15}^{\mathrm{II}} + e_{15}^{\mathrm{I}}k_{\mathrm{I}}\sin\Gamma), \\
F_4 = & -(k_{\mathrm{I}}\sin\Gamma e_{15}^{\mathrm{I}} - e_{15}^{\mathrm{II}}k_{\mathrm{II}}\sin\Gamma_{\mathrm{II}})(k_{\mathrm{II}}\sin\Gamma_{\mathrm{II}}e_{15}^{\mathrm{II}} + e_{15}^{\mathrm{I}}k_{\mathrm{I}}\sin\Gamma) \\
& -(k_{\mathrm{II}}\sin\Gamma_{\mathrm{II}}\kappa_{11}^{\mathrm{II}} - \kappa_{11}^{\mathrm{I}}k_{\mathrm{I}}\sin\Gamma)(c_{44}^{\mathrm{I}}k_{\mathrm{I}}\sin\Gamma + k_{\mathrm{II}}\sin\Gamma_{\mathrm{II}}c_{44}^{\mathrm{II}}), \\
F = & (c_{44}^{\mathrm{I}}k_{\mathrm{I}}\sin\Gamma + k_{\mathrm{II}}\sin\Gamma_{\mathrm{II}}c_{44}^{\mathrm{II}})(k_{\mathrm{II}}\sin\Gamma_{\mathrm{II}}\kappa_{11}^{\mathrm{II}} + \kappa_{11}^{\mathrm{I}}k_{\mathrm{I}}\sin\Gamma) \\
& +(k_{\mathrm{II}}\sin\Gamma_{\mathrm{II}}e_{15}^{\mathrm{II}} + e_{15}^{\mathrm{I}}k_{\mathrm{I}}\sin\Gamma)^2.
\end{aligned}$$

The resulting interfacial stress can be expressed as

$$\tau_{yz}(X,0) = \tau\sin\Gamma_{\mathrm{II}}\mathrm{e}^{-\mathrm{i}k_{\mathrm{II}}X\cos\Gamma_{\mathrm{II}}},$$

where τ is the maximum value of the shear stress corresponding to the transmitted wave given by

$$\tau = -\mathrm{i}k_{\mathrm{II}}(c_{44}^{\mathrm{II}}\overline{w}_{\mathrm{II}} + e_{15}^{\mathrm{II}}\overline{\phi}_{\mathrm{II}}).$$

References

Ashley, S., 1995. Smart skis and other adaptive structures. Mechanical Engineering 76–81.

Dosch, J., Lesieutre, G., Koopmann, G., Davis, C., 1995. Inertial piezoceramic actuators for smart structures. SPIE 2447, 14–25.

Dunn, M., 1994. The effect of crack face boundary conditions on the fracture mechanics of piezoelectric solids. Engineering Fracture Mechanics 48, 25–39.

Gandhi, M.V., Thompson, B.S., 1992. Smart Materials and Structures. London, Chapman & Hall.

He, M.-Y., Suo, Z., McMeeking, R.M., Evans, A.G., Lynch, C.S., 1994. The mechanics of some degradation mechanisms in ferroelectric ceramic actuators. SPIE 2189, 344–356.

Jain, A.K., Sirkis, J.S., 1994. Continuum damage mechanics in piezoelectric ceramics. Adaptive Structures and Composite Materials: Analysis and Application AD 45/MD 54, 47–58.

Li, S., Mataga, P.A., 1996a. Dynamic crack propagation in piezoelectric materials – Part I, electrode solution. Journal of Mechanics and Physics of Solids 44, 1799–1830.

Li, S., Mataga, P.A., 1996b. Dynamic crack propagation in piezoelectric materials – Part II, vacuum solution. Journal of Mechanics and Physics of Solids 44, 1831–1866.

Mal, A.K., Lee, J., 1993. Deformation and stress fields in a composite beam with embedded multiple actuators and sensors. Adaptive Structures and Material Systems AD 35, ASME, 113–116.

McMeeking, R.M., 1989. Electrostrictive stresses near crack-like flaws. Journal of Applied Maths and Physics 640, 615–627.

Narita, F., Shindo, Y., 1998. Scattering of love waves by a surface-breaking crack in piezoelectric layered media. JSME International Journal Series A 41, 40–48.

Pak, Y.E., 1990. Crack extension force in a piezoelectric material. ASME Journal of Applied Mechanics 57, 647–653.

Pak, Y.E., Goloubeva, E., 1995. Influence of cracks on electroelastic properties of piezoelectric materials. Adaptive material systems AMD 206/MD 58, 33–43.

Park, S.B., Sun, C.T., 1994. Crack extension in piezoelectric materials. SPIE 2189, 357–368.

Shindo, Y., Katsura, H., Yan, W., 1996. Dynamic stress intensity factor of a cracked dielectric medium in a uniform electrical field. Acta Mechanica 117, 1–10.

Sosa, H.A., 1991. Plane problems in piezoelectric media with defects. International Journal of Solids and Structures 28, 491–505.

Sosa, H.A., Pak, Y.E., 1990. Three-dimensional eigenfunction analysis of a crack in a piezoelectric material. International Journal of Solids Structures 26, 1–15.

Suo, Z., Barnett, D.M., Wills, J.R., 1992. Fracture mechanics for piezoelectric ceramics. Journal of Mechanics and Physics of Solids 40, 739–765.

Varadan, V.K., Wu, Z., Bao, X.-Q., Varadan, V.V., 1993. Light weight robot using piezoelectric motor, sensor and actuator. Adaptive Structures and Material Systems AD 35, 141–148.

Wang, X.D., Meguid, S.A., 1997. Diffraction of SH-wave by interacting matrix crack and an inhomogeneity. ASME Journal of Applied Mechanics 64, 568–575.

Zhang, T.Y., Qian, C.F., Tong, P., 1998. Linear electro-elastic analysis of a cavity or a crack in a piezoelectric material. International Journal of Solids Structures 35, 2121–2149.